The Journal of Chemical Physics

RESEARCH ARTICLE | OCTOBER 25 2023

Cryo-IR spectroscopy and cryo-kinetics of cluster N_2 adsorbate complexes of tantalum cluster cations Ta_{5-8}^+

Daniela V. Fries ; Matthias P. Klein ; Annika Straßner ; Maximilian E. Huber ; Gereon Niedner-Schatteburg

Check for updates

J. Chem. Phys. 159, 164306 (2023)
https://doi.org/10.1063/5.0157218

View Online
Export Citation

29 April 2024 14:10:59

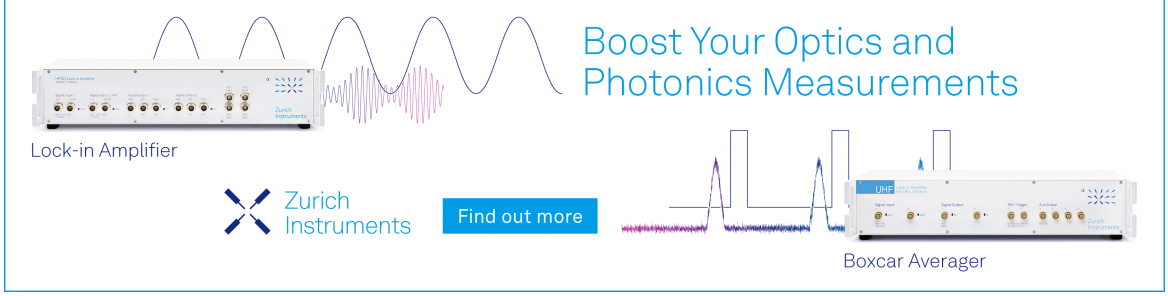

AIP Publishing

The Journal of Chemical Physics ARTICLE pubs.aip.org/aip/jcp

Cryo-IR spectroscopy and cryo-kinetics of cluster N_2 adsorbate complexes of tantalum cluster cations $Ta_{5\text{-}8}^+$

Cite as: J. Chem. Phys. 159, 164306 (2023); doi: 10.1063/5.0157218
Submitted: 5 May 2023 • Accepted: 12 September 2023 •
Published Online: 25 October 2023

View Online Export Citation CrossMark

Daniela V. Fries, Matthias P. Klein, Annika Straßner, Maximilian E. Huber, and Gereon Niedner-Schatteburg[a]

AFFILIATIONS

Department of Chemistry and State Research Center OPTIMAS, Rheinland-Pfälzische Technische Universität (RPTU) Kaiserslautern-Landau, 67663 Kaiserslautern, Germany

[a]Author to whom correspondence should be addressed: gns@rptu.de

ABSTRACT

We present an IR-PD study of tantalum cluster adsorbate complexes $[Ta_n(N_2)_m]^+$, abbreviated (n,m), n = 5–8. We utilize infrared spectroscopy of isolated and size selected clusters as prepared and characterized by a cryogenic tandem ion trap setup, and we augment our experiments with quantum chemical simulations at the level of density functional theory. The cluster adsorbate complexes (n,m) reveal vibrational bands above 2000 cm^{-1}, which indicate end-on coordinated μ_1-N_2 oscillators, and bands below 2000 cm^{-1}, which indicate side-on μ_2-κN:κN,N coordinated ones. We observe a general increase in spectral complexity and an inhomogeneous broadening, mainly towards the red, at certain points of N_2 loading m, which originates from an increasingly higher amount of double and triple N_2 coordination at Ta sites, eventually at all of them. Other than the small tantalum clusters Ta_n^+, n = 2–4, the IR-PD spectra of the initial N_2 adsorbate species (n,1), n = 5–8, provide strong evidence for a lack of spontaneous N_2 cleavage. Spontaneous N_2 cleavage by Ta_n^+, n = 5–8, seems suppressed. Therefore, the ability of a small Ta cluster to cleave dinitrogen disappears with one more tantalum core atom. The study of stepwise N_2 adsorption on size selected Ta_n^+, n = 5–8 clusters revealed adsorption limits $m_{(max)}$ of $[Ta_n(N_2)_m]^+$ that are independent of cluster size within this size range. Cryo-adsorption kinetics at 26 K allowed for kinetic fits to consecutive N_2 adsorption steps, and the fits revealed significant N_2 desorption rates upon higher N_2 loads, and the cluster adsorbate complexes eventually reached equilibrium. Some enhanced N_2 desorption rates point towards likely adsorbate shell reorganization, and there is also some evidence for the coexistence of isomeric cluster adsorbate complexes.

© 2023 Author(s). All article content, except where otherwise noted, is licensed under a Creative Commons Attribution (CC BY) license (http://creativecommons.org/licenses/by/4.0/). https://doi.org/10.1063/5.0157218

29 April 2024 14:10:59

INTRODUCTION

The application of transition metals (TM) in heterogeneous catalysis is the basis for numerous industrial processes.[2–7] Mechanistic understanding of the catalytic reactions was early on postulated to take place at so-called active sites[8] that are part of the solid surface of a catalyst, which is most often less characterized when *in operando*. Transition metal clusters serve as model systems for these active sites in order to provide insights into elemental catalytic processes at the molecular level.[9–15] All of this research elucidates cluster size effects on their structure and on their reactivity.

In particular, there are numerous studies that demonstrate the interaction and reactivity of tantalum clusters and their alloys, carbides and chalcogenides, with small molecules such as N_2,[1,16–23] CH_4,[17,24–26] CO_2,[27] and O_2.[28] Interaction, leading towards adsorption, is understood to yield adsorbates on the cluster surfaces. The cluster adsorbate complexes may act as precursor states for the activation and bond cleavage of these adsorbates. The issue of N≡N bond cleavage, for example, plays a role in the ongoing research efforts to develop an energetically optimized protocol, e.g., for Haber–Bosch NH_3 production, a catalytic process of paramount significance to mankind on this planet and beyond.[29,30]

N_2 activation has also been observed to proceed by small clusters of Co and Rh when assisted by surface plasma radiation,[31,32] and bare TM clusters of V, Gd, and Sc,[33–35] and homo- and heterometallic cluster carbides, with some subsequent C–N bond

© Author(s) 2023

formation,[16,17,36,37] and ultimately through lithiated TM complexes.[38]

Size effects, an intrinsic propriety of clusters, prevail in tantalum clusters as well. The governing thermochemistry drives tantalum cluster cations of six atoms and less to reduce CO_2 to CO, while larger ones form adducts.[27] There are further size effects in the oxidation of such tantalum cluster cations, with the Ta_8^+ cluster cation sticking out by its oxidative cleavage towards $Ta_4O_4^+$.[28] Furthermore, size effects arise from small tantalum clusters (n = 1–4) dehydrogenating CH_4 and concurrently eliminating H_2, yielding the product of the stoichiometry $[Ta_n,C,2H]^+$, while larger clusters (n = 5–10) enable mere molecular adsorption.[26] While the bare Ta_5^+ cluster is inert towards CH_4, its monoxide, Ta_5O^+, activates CH_4.[24]

The elucidation of such size effects asks for a structural characterization of participating species that may arise through spectroscopic experiments, which elucidate characteristic vibrations of, e.g., cluster adsorbate complexes and eventual reaction products.

Historically, inelastic electron scattering off N_2 layered surfaces has proved valuable, but it has suffered from limited spectral resolution.[39,40] The technical advancement of infrared photon dissociation (IR-PD) spectroscopy by either free electron lasers (FEL) or Optical Parametric Oscillator (OPO) technology has helped to identify characteristic vibrational bands, in particular when applied to isolated clusters and their complexes, and thereby achieve sufficient spectral resolution (as low as ±5 cm^{-1}),[41–44] and this method is widely applicable and well established by now.[45–54]

In any case, it is mandatory to augment recorded vibrational spectra with quantum chemical modeling by density functional theory (DFT) methods in order to enable sound structural and dynamic interpretation. A successful example of such an approach is, e.g., the subsequent elucidation of the afore-mentioned tantalum product complex $[4Ta,C,2H]^+$[24] by IR-MPD spectroscopy and first principles quantum calculations, which identified a dihydride carbide formation, $H_2Ta_4C^+$, and ruled out any other CH bond containing species.[25] Another study complements experimental results from vibrational spectra and theoretical modeling of bare Ta_n^+ clusters, n = 6–20, and it managed to identify cluster geometries, their relative stabilities, and electronic properties.[55,56] An early study on the chemisorption properties of small tantalum clusters has revealed an oxygen adatom effect on the N_2 uptake rate.[18] Several studies including DFT modeling of small tantalum clusters provide strong evidence for dissociative N_2 adsorption.[19–23,57] A 2022 perspective summarizes recent progress in the field of nitrogen activation by TM species in the gas phase, and it shows that a systematic understanding of cluster reactivity towards N_2 is lacking to date.[58]

With this work, we build on our earlier study of Ta_4^+[1] and complement it with a study of cationic clusters of n = 5–8 tantalum atoms. We reacted the bare clusters with N_2 at 26 K and recorded IR-PD spectra of the adsorption species $[Ta_n(N_2)_m]^+$, similar to our earlier studies on Ni_n^+, Rh_n^+, $Rh_iFe_j^+$, and Fe_n^+ clusters.[59–64] In the adjoined IR-PD study [**IRS1**], we discuss the N_2 adsorption onto the three small clusters $Ta_{2\text{-}4}^+$. In our current study [**IRS2**], we actually present findings for the N_2 adsorption onto the cluster sizes $Ta_{5\text{-}8}^+$. The findings of both studies, which we refer to in the following as [**IRS1**] and [**IRS2**], respectively, find strong support through our complementary cryogenic kinetic study (cf., supplementary material). The combination of IR-PD measurements and DFT modeling with kinetic studies provides insights into the structures of the N_2 adsorbate species (5,m), (6,m), (7,m), and (8,m). We gain insight into the coordination motifs of the N_2 ligands and find strong size effects, especially in terms of the first few adsorbates. We clarify and extend the overall picture and provide a systematic study of N_2 adsorption on small tantalum clusters Ta_n^+, n = 2–8. While we find complete cleavage of the N_2 triple bond of the very first adsorbed N_2 molecule on Ta_2^+, Ta_3^+, and Ta_4^+, the present study provides strong evidence for a lack of cleavage for clusters from Ta_5^+ on and beyond. Instead, adsorption of the first N_2 molecule occurs in end-on orientation to the cluster core exclusively.

EXPERIMENTAL AND COMPUTATIONAL METHODS

It is a tandem cryo-ion trap instrument that serves as the platform for all of the experiments conducted. It consists of a customized Fourier transform ion cyclotron resonance (FT-ICR) mass spectrometer (Apex Ultra, Bruker Daltonics) that encompasses cluster ion generation, size selection, N_2 coordination, cluster adsorbate complex selection, and eventually infrared photon dissociation (IR-PD) spectroscopy of the respective cluster adsorption species. Note that this protocol comprises an MS^3 procedure. Detailed descriptions of the ion generation and adsorption processes of the metal clusters can be found elsewhere[1,59,60,64–67] and also in the supplementary material, where we present and discuss adjoined kinetic studies.

Briefly, we trap the cluster ions in an RF hexapole ion trap using the routine described in Text S3 in the supplementary material and guide the thus generated cluster N_2 adsorbate complexes into the cryogenic (~10 K) FT-ICR cell. For recording IR-PD spectra, we trap and select each cluster adsorbate species of interest in the IRC cell and irradiate each isolated ion packet by a tunable IR laser system with 7–10 laser pulses with an energy of 0.5–3.0 mJ each. These IR photon pulses stem from a pulsed injection seeded Nd:YAG laser (10 Hz, PL8000, Continuum), which pumps a KTP/KTA optical parametric oscillator/amplifier (OPO/OPA, LaserVision). An $AgGaSe_2$ crystal generates the difference frequency (DF) of the OPA's signal and the idler waves, whereby we generate the applied IR irradiation in the range of 1100 and 2400 cm^{-1}. Absolute values of the DFM frequencies were derived from the online monitored OPO signal frequencies (continuous online wavemeter monitoring, *Bristol Instruments*, 8721B-NIR) and the pre-recorded value of the Nd:YAG frequency. Fragmentation mass spectra are recorded during continuous scans of the IR wavelength, and the recorded IR-PD signal transforms into a fragmentation efficiency via evaluation of $\frac{\sum_i F_i}{\sum_i F_i + \sum_i P_i}$, where F_i and P_i are fragment and parent ion intensities. The plotted fragmentation efficiency as a function of laser frequency finally yields the IR-PD spectrum. In all cases, single or multiple N_2 losses were the only observed fragmentation channels.

Quantum chemical modeling by Density Functional Theory (DFT) served to obtain optimized cluster (adsorbate) geometries and vibrational eigenmodes, as achieved by the program packages Gaussian 09 and 16.[68,69] We employed the hybrid functional PBE0[70,71] along with the Def2-TZVP basis set[72,73] for all atoms in (5,0) cases, the Def2-TZVP basis set[72] for N atoms, and the cc-pVTZ-pp basis set[74] for Ta atoms in all (6,m) and (7,m) cases. We did so in continuity with prior studies that have succeeded to model N_2

29 April 2024 14:10:59

© Author(s) 2023

adsorption before[60,61,64,66,67]—particularly for the adsorption, activation, and cleavage of N_2 on Ta_4^+ clusters.[1] We tolerated relaxed SCF convergence criteria of 10^{-6} (as compared to 10^{-8} in "standard" DFT calculations) in order to achieve swift SCF convergence. The vibrational eigenmode spectra of all optimized geometries were inspected for the absence of any imaginary frequency. We applied optimized scaling factors of 0.9586 and 0.9512 for (6,m) and (7,m), respectively, for the cluster sizes to account for the prevailing anharmonicities, documenting unscaled IR frequencies in the supplementary material. We arrive at theoretical IR absorption spectra by convolution of the predicted and scaled IR frequencies with a Gaussian profile of FWHM = 5 cm^{-1}. Natural Population Analysis (NPA) was performed via the NBO 5.9 option as implemented in Gaussian 09.[75]

RESULTS AND DISCUSSION

The current IR-PD spectroscopic study of the N_2 adsorbates of Ta_n^+ clusters, n = 5–8, was conducted under adiabatic conditions, and it is complemented by some N_2 adsorption kinetics studies (cf. supplementary material). Here, we extend and complete our IR-PD study on the small cluster adsorbates (n,m), n = 2–4, as discussed in the adjoined infrared study [**IRS1**]. Once more, we recorded IR-PD patterns that vary remarkably by the size of the Ta_n^+ clusters, n, which in turn vary by the amount of N_2 adsorbate, m. In keeping with the adjoint study [**IRS1**], we arrange the studied cluster adsorbates in a (n,m) matrix and discuss the respective IR-PD spectra of each cluster size n in separate chapters.

The adsorbed N_2 chromophores in each of the cluster adsorbate complexes possess vibrational bands, which we record as IR-PD features. Therefore, for all cluster adsorbate complexes (n,m) studied, we observe a specific and individual variation of IR-PD features as a function of the tantalum cluster size n and the nitrogen adsorbate loading m. In all cases, the recorded N_2 fingerprint features range from 2000 to 2350 cm^{-1}, and they most likely correspond to end-on N_2 adsorbates that coordinate in a μ_1 fashion to individual tantalum centers, with little to no interaction with other neighboring tantalum centers. This interpretation is in line with previously reported cases for Fe_n^+,[64] Co_n^+,[65] Ni_n^+,[59,60] Ru_n^+,[66] Rh_n^+,[67] and even Ta_4^+.[1] In addition to these end-on bands, there are some cases where we observe IR-PD bands in the range of 1300–1700 cm^{-1}, which indicate the most likely presence of a side-on μ_2-κN:κN,N N_2 ligand within the respective cluster adsorbate complex. This conclusion follows from the results of our previous study of N_2 on a Ta_4^+ cluster.[1]

$[Ta_5(N_2)_m]^+$

We recorded IR-PD spectra of all cluster adsorbate complexes from (5,1) up to (5,13) (Fig. 1). We observe bands in the end-on N_2 stretching range at 2000–2300 cm^{-1} for all investigated cluster adsorbate complexes, while there are little and weak IR-PD bands in the side-on N_2 range below 2000 cm^{-1}. There are IR-PD signals in the end-on N_2 stretching range at all levels of N_2 adsorption, m = 1–13. There is no indication for N_2 activation and nitride formation whatsoever. While Nitride formation would be highly exothermic (cf. Table S3 in the supplementary material), the recorded IR-PD signatures signify intact N_2 adsorbates, and it seems to prevail an extensive kinetic hindrance by unsurmountable barriers. If activated

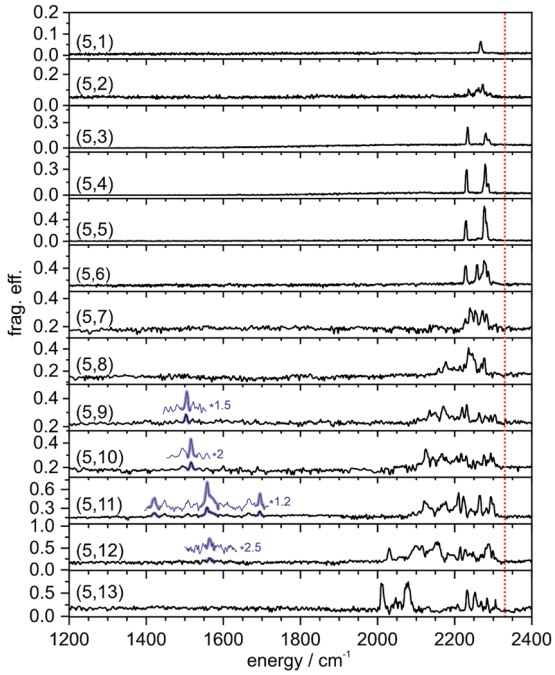

FIG. 1. IR-PD spectra of sequentially increasing cluster N_2 adsorbate complexes $[Ta_5(N_2)_m]^+$, m = 1–13, as recorded after prior 26 K He buffer gas cooling. Note the significant red-shift of the IR-PD bands with respect to the free N_2 stretching vibrational frequency (2330 cm^{-1},[76] red dotted line).

nitrides form at all, they seem to be minor and leave no fingerprint. Instead of N_2 cleavage, we find a manifold of bands that persist at any level of N_2 adsorption and shift slightly to the red with increasing N_2 adsorption. In parallel, at (5,8) and beyond, we observe some broad and some sharp bands appearing to the red and spreading out to almost 2000 cm^{-1}. It seems appropriate to account for the observed redshifts with respect to the free N_2 stretching vibration at 2330 cm^{-1} in terms of a σ-donor and π-acceptor synergism as before. Up to species (5,8), we found no evidence of a N_2 stretching vibrational band in the side-on range. For species (5,9) to (5,12), the IR-PD spectra indicate the presence of some weak adsorptions in the range between 1400 and 1700 cm^{-1}. In the following, we will briefly discuss the recorded IR-PD spectra (5,m) and some of their IR-PD bands in some more detail.

For single N_2 adsorption m = 1, (5,1), we found a sharp single band at 2268 cm^{-1}, which is red-shifted by 62 cm^{-1} with respect to the free N_2 stretching vibration at 2330 cm^{-1}.[76] The (5,2) spectrum shows a more complex IR-PD band pattern, and we identify bands at 2236, 2257, 2262, and 2273 cm^{-1}. Instead of merely two bands, e.g., from a single isomer with two end-on coordinated N_2 molecules, we observe a manifold of at least four weak bands between 2200 and 2300 cm^{-1} and thus conclude on some co-existing isomers with comparable stabilization energies. The recorded IR-PD spectra of the species (5,3), (5,4), and (5,5) reveal no significant changes, and we observe three bands: An intense single band shifts slightly to the red from 2234, (5,3), to 2229 cm^{-1}, (5,5); another intense band shifts to the red from 2281, (5,3) to 2277 cm^{-1}, (5,5). Finally, there is

29 April 2024 14:10:59

© Author(s) 2023

another weak band at 2289 cm^{-1} (5,3) that shifts less with increasing m and thus merges into a mere shoulder of the second band in the IR-PD spectrum (5,5) (2282 cm^{-1}). The slight redshift of the measured IR-PD bands with m cross-references to our prior studies on the N_2 adsorption to other transition metal clusters such as Fe_n^+[64] and Ni_n^+.[59] In both cases, we found similar effects, and we took them as an indication of rough cluster surfaces. The adsorption of one and two more N_2 molecules onto the formal monolayer at (5,5) yields a more complicated IR-PD band pattern for species (5,6)—and even more so for (5,7). The prior (5,5) IR-PD spectrum is augmented by one more band at 2259 cm^{-1} in (5,6) and another band on top at 2240 cm^{-1} in (5,7). The spectral broadening continues through the adsorption of the eighth N_2 molecule, and the recorded IR-PD bands for (5,8) stretch out across a significantly wider range, from 2150 to 2300 cm^{-1}. Nevertheless, we identify some partially resolved maxima at 2159, 2177, 2214, 2225, 2236, 2241, 2246, 2252, 2269, and 2277 cm^{-1}. The new, most red-shifted bands might arise either from a variation of Ta center next neighbor coordination or from a triple end-on N_2 occupation at a single Ta center. The IR-PD spectra of (5,9), (5,10), and (5,11) largely resemble that of (5,8), and we observe broad IR-PD patterns spread out across 2130–2310 cm^{-1}, with some IR-PD bands partially resolved. The observed excess of IR-PD bands over present N_2 oscillators clearly indicates co-existing isomers, which likely differ in the very structure of the N_2 adsorbate shell or less likely differ in some parameters of the relaxed cluster core. In contrast to the prior IR-PD spectra, the spectra of the three species (5,9), (5,10), and (5,11) reveal a weak IR-PD band at 1504, 1516, and 1558 cm^{-1}, respectively, which indicates the most likely presence of a side-on μ_2-κN:κN,N N_2 ligand. In addition, (5,11) reveals two more bands at 1422 and 1694 cm^{-1} that indicate further side-on N_2 coordination at other sites and with varying coordination parameters such as, e.g., the tilting angle. The IR-PD spectra of species (5,12) and (5,13) reveal another increase in the maximum of redshifts and an eventual gain in spectral structure and reduction of broadening. In (5,13), the end-on coordinated N_2 ligands seems to separate into two classes, as indicated by high and low redshifted bands at 2010–2080 cm^{-1} and 2208–2306 cm^{-1}, with less to no options in between other than before. A side-on μ_2-κN:κN,N N_2 indicating band of (5,12) at 1563 cm^{-1} continues the trend of such bands in (5,9) – (5,12), and it terminates this series, as (5,13) does not reveal any such or similar IR-PD signal. It seems as if at this point the shell of N_2 adsorbates has become so sterically crowded that a two Ta center coordinating N_2 tilt is not possible anymore. Instead, the lack of wagging space leads to an increase in stiffness in this N_2 adsorbate shell, which might manifest in a highly structured and well-resolved IR-PD spectrum of (5,13).

In summary, we found numerous IR-PD bands in the IR-PD spectra of species (5,m), m = 1–13, which are located mainly in the end-on coordinated N_2 stretching range of 2000–2310 cm^{-1}. Some of these species (m = 9–12) indicate weak IR-PD signals below 2000 cm^{-1}, which we assign to side-on μ_2-κN:κN,N N_2 ligands. Starting with a few single and distinguishable end-on N_2 bands of the less occupied species (5,m), m small, we observe with increasing m an overall increase of spectral complexity and an asymmetric broadening, largely towards the red. Finally, the spectrum of (5,13) reveals some sharp bands. While intermediate N_2 loads (moderate m values) allow for much spectral complexity and likely isomerism, the highly loaded species with much of a filled N_2 shell exhibit reduced spectral complexity and less isomerism. This indicates the onset of orientational stiffness and a less wagging disorder. Side-on μ_2-κN:κN,N N_2 coordination seems to die out.

Other than the smaller tantalum clusters Ta_n^+, n = 2–4 (cf. Fries *et al.*[1] and the adjoined study [**IRS1**]), the (5,m) spectra provide strong evidence for a lack of any spontaneous N_2 cleavage. Note that we found IR-PD fingerprints of end-on bound N_2 molecules on otherwise bare Ta_5^+ clusters and a lack of side-on μ_2-κN:κN,N N_2 fingerprints. It appears as if an enhanced entrance channel barrier prevents spontaneous tilting and further activation. It takes further N_2 adsorption to find some weak side-on μ2-κN:κN,N N_2 fingerprints. Spontaneous N_2 cleavage by Ta_5^+ seems suppressed.

In order to investigate the effects of stepwise N_2 adsorption on the cluster structure and possible spin relaxations in the course of adsorption, we optimized the Ta_5^+ cluster core together with the adsorbate shell of (5,m) in the cases of m = 0,1,2,5,10 comprising end-on N_2 ligands. For each m, we started with several conceivable adsorption shell isomers, which adsorb N_2 onto a reasonable trigonal bipyramid (tbp) cluster framework. We obtained fully converged structures for singlet to nonet multiplicities in most cases (Fig. 2). Vertical offsets of the (5,m) curves depict N_2 adsorption and desorption energies—each of these curves resembling the spin valley[61] of a single (5,m) complex. We find triplet and singlet isomers most stable in all cases and sometimes almost degenerate.

The bare Ta_5^+ cluster finds itself most stable in a triplet trigonal bipyramidal (tbp) minimum structure ^{3}tbp, independent of starting geometries. Two apical Ta atoms coordinate three next neighbors each, and the three equatorial Ta atoms coordinate four next neighbors each. This most stable isomer is close to D_{3h} symmetry. The singlet electromer is slightly less stable, by a mere 14 kJ/mol. Higher multiplicities are more expensive by at least 90 kJ/mol and much

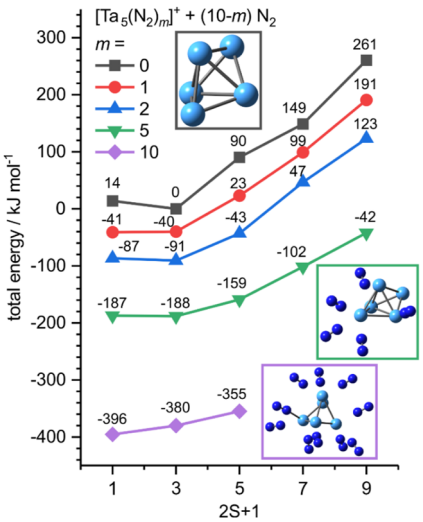

FIG. 2. Total energies of computed $[Ta_5(N_2)_m]^+$ cluster adsorbate complexes (5,m) as a function of the spin multiplicity 2S + 1, and normalized to the most stable (5,0) spin isomer (trigonal bipyramid, 3tbp, triplet). The calculated minimum structures for (5,0), (5,5), and (5,10) are shown as insets; the geometries of other multiplicities may differ slightly.

29 April 2024 14:10:59

© Author(s) 2023

beyond. Through single N_2 adsorption, singlet and triplet multiplicities become degenerate. This degeneracy persists throughout further N_2 adsorption, up to m = 5. Note that high multiplicities seem to stabilize as well, and the spin valleys become more shallow. The energy difference between each curve's minimum and the quintet state decreases from 63 kJ/mol (m = 1) over 48 kJ/mol (m = 2) to 29 kJ/mol (m = 5).

The most stable (5,5) cluster adsorbate complex has its N_2 adsorbate shell concentrating on one side of the tbp cluster core: two of the equatorial Ta atoms are singly occupied, and one of the two apical Ta atoms has adsorbed three N_2 molecules. Upon adsorption of ten N_2 molecules, yielding the most stable (5,10) cluster adsorbate complex, the tbp cluster core has received some significant distortion towards an oblate geometry. Two opposite (apical) Ta atoms adsorb only a single N_2 molecule. Two other Ta atoms adsorb a triplet of N_2 molecules each. In (5,10), the singlet state is favored over the triplet state by 16 kJ/mol. We thus assume that adsorption-induced spin quenching could occur at high N_2 coverage, m ≥ 5.

We extract adsorption energies from the spin valley curves by evaluating their offsets, which yield both vertical (spin conserving) and adiabatic (including relaxation of the spin state) adsorption energies (cf. Fig. S2 and Table S2). In most cases, the vertical and adiabatic energies are very similar, as singlet and triplet states are close to degenerate. The adsorption energies increase from about −40 kJ/mol (m = 0) to about −50 kJ/mol (m = 1), irrespective of multiplicity. From m = 2 to m = 4, we interpolate values of about −32.4 kJ/mol per N_2 adsorbate. From m = 5 to m = 9, we interpolate adiabatic adsorption energies of −41.5 kJ/mol per N_2, which are slightly larger than the vertical ones (−38.4 kJ/mol per N_2).

Through natural population analysis (NPA), we obtained more information on the charge and spin distributions of some selected clusters and on the influence of the first N_2 adsorption.

The NPA of the most stable (5,0) ^{3}tbp isomer reveals a concentration of the positive charge on the equatorial Ta atoms (Fig. S4). The two apical Ta atoms possess less positive charge density and more spin density than the three equatorial ones. A spin density of ~1 at each of the two apical Ta atoms indicates the localization of a single unpaired electron at each of them.

All of the three considered (5,1) isomers a, b, and c (Fig. S5) are tbp type structures, and they are equally stable (within the uncertainty of the DFT modeling, about 4 kJ/mol), with all other structures being less stable by +18 kJ/mol and beyond. The isomers a, b, and c reveal minor changes in singlet or triplet spin preference and in the predicted orientation of the end-on coordinated N_2 adsorbate. In effect, isomers a and b find themselves in close proximity to C_S symmetry, whereas c possesses C_{2v} symmetry. Their computed linear absorption spectra are depicted in the supplementary material, Fig. S3. Application of the successfully applied scaling factor of our prior Ta_4^+ study (see the adjoined study [**IRS1**]) 0.9736 finds isomer b interpreting the recorded IR-PD spectrum well, isomer a less likely, while isomer c may be ruled out. These assumptions find nice correspondence in the spin valley prediction—^{1}(5,1) is slightly less stable than ^{3}(5,1)—and in structural motifs of N_2 coordination to TM centers such as Rh and Ta, where we found a preferred "90° to surface normal" N_2 coordination that persists for many species along the adsorption chain.[1,77]

As in the naked (5,0) Ta cluster, the (5,1) N_2 adsorbate complex locates a large fraction of positive charge on the three equatorial Ta atoms and the majority of electron density in triplet states at the two apical Ta atoms. Note that the N_2 molecule prefers to adsorb onto either of the three equatorial Ta atoms, which serve as better electron acceptors than the two apical ones.

In the case of the triplet isomers b and c, both apical Ta atoms comprise an unpaired electron each, and their charge density is reduced with respect to the singlet isomer a by 0.04*e* per Ta atom. Upon adsorption, the N_2 molecule is polarized ($\Delta q < 0.29e$) but obtains little net charge and little net spin density. The electron population of the adsorbing Ta atom strongly depends on the isomer (spin and mainly angle), in particular if compared with the other equatorial Ta atoms: it varies between 0.255, b, and 0.174*e*, c. In the singlet isomer a, the adsorbing Ta atom is the most positive equatorial atom with a charge density of 0.255*e*. The charge density of the adsorbing Ta atom in triplet isomer b is in between the other equatorial atoms $0.219e < 0.259e < 0.279e$. In the highly symmetric triplet isomer c, the adsorbing isomer comprises the least charge density of the equatorial Ta atoms ($0.174e < 0.26e$).

In summary, the observed weak IR-PD bands below 2000 cm^{-1} of several species (5,m), m ≥ 9, indicate isomers that might contain a side-on coordinated μ2-κN:κN,N N_2 ligand. However, the measured IR-PD spectra for the adsorbate species (5,m) provide no evidence for N_2 cleavage. We found IR-PD bands of end-on-bound N_2 molecules to single Ta centers for all species along the adsorption chain. It is remarkable, that the addition of a single metal atom to the Ta_4^+ cluster framework eliminates the ability of the cluster to cleave N_2 molecules.

We speculate that the adsorption of a single N_2 molecule induces little change in the electron distribution within the Ta_5^+ cluster core, likely the computed isomer b, and it has almost no effect on the spin density distribution. These effects are specific for each coordination isomer of the (5,1) complex, and they depend strongly on the orientation of the adsorbed N_2 molecule. It remains to elucidate how this changes along the further N_2 adsorption chain.

$[Ta_6(N_2)_m]^+$

Next, we inspect in detail the IR-PD spectra of the tantalum cluster adsorbate species $Ta_6(N_2)_m^+$: (6,m), m = 1–15. We took IR-PD spectra for (6,m) in the 1200–2400 cm^{-1} range (cf. Fig. 3), as we did before for smaller tantalum clusters. That is, we analyzed each adsorbate species for IR-PD vibration bands in the end-on region above 2000 cm^{-1} and in the side-on region below 2000 cm^{-1}. The recorded IR-PD spectra reveal an end-on N_2 fingerprinting fragmentation signal in all investigated cases (6,m) up to m = 15–even for the very first N_2 adsorbate species (6,1). All of these bands are shifted to the red with respect to the stretching frequency of free N_2 at 2330 cm^{-1},[76] but by varying amounts. All of these shifts originate from an interplay of σ-donor and π-acceptor interactions at work, and in a cluster size modulated manner.

In the following, we briefly discuss the recorded IR-PD spectra (6,m) (cf. Fig. 3) and the obtained characteristic bands separately. The IR-PD spectrum of (6,1) reveals merely a single weak IR-PD induced fragmentation at 2293 cm^{-1}. The presence of this IR-PD band reveals strong evidence for a lack of N_2 cleavage on the Ta_6^+ cluster. This is well in line with the observed lack of N_2 cleavage by

29 April 2024 14:10:59

© Author(s) 2023

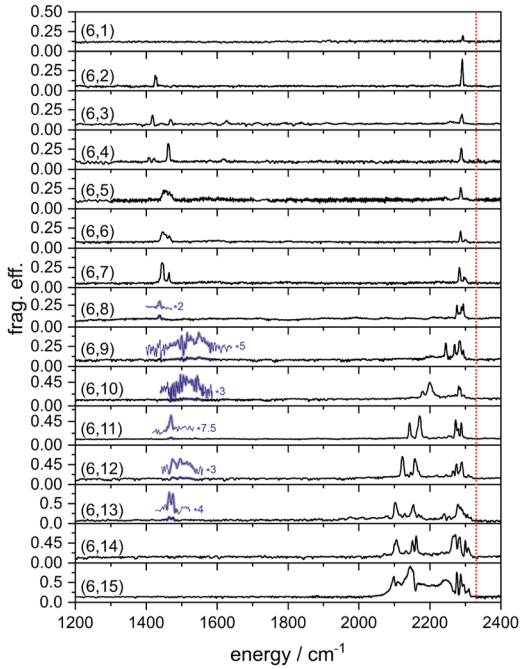

FIG. 3. IR-PD spectra of sequentially increasing cluster N_2 adsorbate complexes $[Ta_6(N_2)_m]^+$, m = 1–15, as recorded after prior 26 K He buffer gas cooling. Note the significant red-shift of the IR-PD bands with respect to the free N_2 stretching vibrational frequency (2330 cm^{-1},[76] red dotted line).

Ta_5^+, which makes for a trend: the N_2 cleavage ability of small tantalum clusters vanishes upon an increase in cluster size. Finally, there is no IR-PD evidence for tilted N_2 side coordination in (6,1).

The IR-PD spectrum of (6,2) reveals a single band at 1425 cm^{-1} and another one at 2292 cm^{-1}. The former one is in accordance with similar bands of smaller tantalum clusters, which we assigned to N_2 molecules acting as μ_2-κN:κN,N ligands that bind side-on across a Ta–Ta edge of the cluster cores. Our DFT calculations will confirm this interpretation, the presence of a single side-on N_2 ligand in the (6,2) complex (cf. below). The other IR-PD band of (6,2), above 2000 cm^{-1}, corresponds to a like band in (6,1), and we assign it to the N_2 stretching vibration of the other N_2 adsorbate, which binds end-on to single tantalum centers.

The IR-PD spectrum of (6,3) reveals evidence for the onset of co-existing adsorption isomers: There are three IR-PD bands in the side-on range, at 1416, 1468, and 1625 cm^{-1}, and a strong band in the end-on range, at 2289 cm^{-1}, with an additional weak and broad IR-PD induced adsorption at 2255 cm^{-1}. Therefore, the number of IR-PD bands (6,3) exceeds the amount of adsorbed N_2 molecules. We interpret this necessarily as strong evidence for the co-existence of adsorbate isomers in a cluster adsorbate complex with a persistent Ta_6^+ cluster core framework. This would be similar to our findings for N_2 adsorbate complexes of the Ta_4^+ (cf. [**IRS1**]) and Ta_5^+ clusters. The IR-PD spectrum reveals a wide spread of IR-PD bands in the side-on range, from 1400 to 1650 cm^{-1}. This reminds us of the Ta_4^+ case in our adjoined study [**IRS1**], where we assigned some observed bands with a diminished redshift to N_2 complexes with a smaller tilt of the side-on μ_2-κN:κN,N N_2 ligand. Therefore, we speculate on multiple isomers, each of which contains a single side-on μ_2-κN:κN,N N_2 ligand across an edge of the cluster core and which likely differ slightly in the degree of tilting. However, co-existing isomers that contain two of these side-on μ_2-κN:κN,N N_2 ligands are conceivable as well. The subsequent DFT calculations will help to clarify.

We observe five distinguishable IR-PD bands for species (6,4): four of them are located in the side-on range at 1406, 1423, 1462, and 1620 cm^{-1} (weak), and a single one is located at 2289 cm^{-1} in the end-on range. Note that the integrated IR-PD signals of the side-on region (below 2000 cm^{-1}) exceed those of the end-on region for all species (6,3) to (6,7), whereas it is the other way around for all cluster adsorbate species with N_2 loads as in (6,8) and beyond.

The IR-PD spectrum of (6,5) comes somewhat as a surprise: it reveals merely two bands, one of which is significantly broadened, around 1448 cm^{-1}, and the other is a sharp IR band at 2287 cm^{-1}, the latter one known as an end-on coordinated N_2 ligand, as observed in all spectra of less loaded clusters. There are little to no shifts with respect to the equivalent bands of (6,4). The broadening of the side-on peak suggests the presence of multiple coordination isomers of two or up to three side-on coordinated N_2 ligands.

The IR-PD spectrum of (6,6) resembles very much that of (6,5), with merely an additional weak band at 2300 cm^{-1}. This new band is located 14 cm^{-1} to the blue of the persistent N_2 end-on band, which might signify a splitting that originates from two N_2 oscillators and their symmetrically/asymmetrically coupled stretching vibrations. Note that our prior investigations of related species have ongoingly found such effects in N_2 adsorbates to other types of transition metal clusters.[59,64] The broad adsorption below 2000 cm^{-1} persists, as observed in (6,5).

The IR-PD spectrum of species (6,7) shows a similar band pattern as (6,6). However, the side-on region of (6,7) yields two well separate bands at 1445 and 1464 cm^{-1}. The ratio of integrated IR-PD signals in the side-on region to those in the end-on region indicates once again a strong contribution of side-on coordinated N_2 chromophores, two or three of them in total.

The side-on IR-PD signal diminishes significantly in (6,8), with a single weak adsorption at 1438 cm^{-1}. In contrast, the IR-PD signal in the end-on range builds up and reveals a strong quartet at 2276, 2284, 2289, and 2294 cm^{-1}, which might either signify various types of symmetric/asymmetric couplings or distinguishable coordination sites and motifs. In any case, all of these IR-PD bands are located in the same frequency range (2250–2300 cm^{-1}) as the singlet and doublet bands of the less loaded adsorbate species.

Starting with the adsorption of the ninth N_2 molecule, the range of observed end-on IR-PD bands widens to the red; in (6,9), it extends down to 2200 cm^{-1}. Features of (6,8) largely persist in (6,9) through three partially overlapping bands at 2269, 2283, and 2294 cm^{-1}. Two new features arise: a sharp band at 2245 cm^{-1} and a further red-shifted broad adsorption around 2202 cm^{-1}. There is a significant change in the IR-PD signal in the side-on range: any discernible IR-PD signal of (6,9) diminishes to some very weak and widely broadened signal around 1525 cm^{-1}, which is less to the red than the intensive peaks of the less loaded species (6,2) to (6,7).

The IR-PD spectrum of species (6,10) merely hints at some broad and very weak adsorption in the side-on range that is hardly discernible and might peak around 1515 cm^{-1}. On its own, this

29 April 2024 14:10:59

© Author(s) 2023

feature might be questionable. Similar broad IR-PD bands in (6,9) and (6,11) lend some credibility to our speculation. In the end-on region, the weak band of (6,9) at 2202 cm^{-1} rises to a prominent doublet of (6,10) at 2180 and 2199 cm^{-1}. Quite the opposite, the four strong bands of (6,9) above 2200 cm^{-1} reduce to a single band of (6,10) at 2283 cm^{-1}.

The observable IR-PD signal of (6,11) in the end-on range broadens to the red and extends from 2140 to 2300 cm^{-1}. There are five distinguishable IR-PD bands at 2143, 2171, 2273, 2280, and 2288 cm^{-1}. The side-on spectral range of the recorded IR-PD spectrum of (6,11) reveals a weak but sharp adsorption at 1470 cm^{-1}, which hints towards a single (6,11) isomer with a side-on μ_2-κN:κN,N coordinated N_2 ligand.

The IR-PD spectra of species (6,12) and (6,13) reveal band patterns that are most similar to those of (6,11). Some IR-PD bands of end-on coordinated N_2 stretching modes reach out slightly further to the red, down to 2100 cm^{-1}. The weak side-on adsorption at 1474 cm^{-1} persists in (6,12), as observed in (6,11), and it reveals a small but discernible splitting in (6,13).

In the IR-PD spectrum of species (6,14), there are no IR-PD bands in the side-on range below 2000 cm^{-1}, and despite a sufficient signal-to-noise ratio. This indicates that the addition of the fourteenth N_2 molecule suppresses any side-on μ_2-κN:κN,N N_2 ligand, and it likely converts any prior one. We speculate that spatial crowding of the many ligands may well favor the slimmer end-on N_2 coordination over the space consuming side-on N_2 coordination. In the IR-PD region of end-on N_2 coordination, above 2000 cm^{-1}, we observe numerous resolved IR-PD bands: 2100, 2106, 2133, 2151, and 2161 cm^{-1}, as well as at 2266, 2272, 2284, 2300, and 2308 cm^{-1}. All in all, these bands are significantly better resolved than in the spectra of (6,12) and (6,13). We take this as a hint towards a reduced degree of disorder in N_2 wagging coordinates.

Reaching out for feasibility limits, we managed to record an IR-PD spectrum of species (6,15). This spectrum revealed numerous IR-PD bands at the end-on coordinated N_2 stretching range above 2000 cm^{-1}. We observe intensive adsorptions at 2098, 2108, 2145, 2276, 2287, 2295, and 2310 cm^{-1}. Moreover, there are some broad IR-PD absorptions without resolved structures between 2168 and 2245 cm^{-1}. It appears as if the fifteenth N_2 ligand induces some enhanced couplings towards and among the other N_2 ligands. This might be well understood in terms of threefold N_2 coordinated Ta centers. At medium N_2 load, m = 9–14, there are one or two such centers, and they may assume distal positions in the octahedral Ta scaffold. Any third center with a threefold N_2 load must, of course, come close to either of the previous ones. Which induces many opportunities for inter-center N_2 stretching mode couplings. In effect, the recorded IR-PD spectrum yields broad and largely unstructured bands—as observed and on display in the (6,15) spectrum of Fig. 3.

In summary, we found numerous IR-PD bands in various wavenumber ranges for the N_2 adsorption species (6,m), m = 1–15, mainly in the range of 1400–1650 cm^{-1} and 2000 to 2310 cm^{-1}. We assign the discernible IR-PD bands below 2000 cm^{-1} to side-on bound μ_2-κN:κN,N N_2 molecules and those above 2000 cm^{-1} to μ_1 end-on coordinated N_2 molecules. The end-on bound N_2 coordination signature in (6,1) corresponds to a similar finding in (5,1). Therefore, Ta_6^+ provides strong evidence for a lack of any spontaneous N_2 cleavage as well. For some species, explicitly (6,3) and (6,4), the total number of IR-PD bands exceeds the total number of N_2 adsorbates, which provides strong evidence of coordination isomers. The μ_1 coordination dominates the end-on range of the IR-PD spectra at low N_2 loads up to m = 5. With increasing N_2 coverage, we observe an overall asymmetrical spread out to the red of the end-on bands. At the highest recorded N_2 load, in the IR-PD spectrum of (6,15), the end-on bands assume a range of more than 200 cm^{-1}, between 2100 and 2310 cm^{-1}. We attribute the observation of such a wide spreading out to an increasingly higher amount of double and triple N_2 coordination at Ta sites of the cluster scaffold, eventually at all of them. The higher the N_2 coordination of Ta, the more the vibrational frequencies of the corresponding N_2 ligands shift to the red.

The side-on μ_2-κN:κN,N N_2 coordination motifs emerge in most of the IR-PD spectra, except (6,1), (6,14), and (6,15). At low N_2 loads, up to (6,7), the side-on fingerprints are roughly as strong as the end-on ones. At high N_2 loads (6,8) and beyond, there is an undisputable propensity for favorable end-on signatures, and side-on ones diminish. Therefore, it appears as if highly loaded clusters prefer, upon saturation, an exclusive end-on N_2 coordination, and partially loaded ones enable a mixture of some side-on N_2 coordination with some end-on N_2 coordination. Steric overcrowding seems to enforce the spatially less demanding end-on N_2 coordination in (6,14) and (6,15).

We undertook DFT modeling for conceivable clusters (6,m) in order to investigate the structure and geometry of the bare Ta_6^+ cluster (m = 0) and its first N_2 adsorbate species up to m = 3.

We found the bare Ta_6^+ cluster most stable in a slightly compressed octahedral structure, with four slightly elongated equatorial bonds (cf. Table S9) and a doublet state (M = 2). We also found some less stable structure, a nido-pentagonal pyramid with a quartet state (M = 4, +66 kJ/mol). Other test structures were optimized into either of these two. Energetics of other spin states/multiplicities and further details are to be found in the supplement (cf. Table S4). Our present conclusions on the naked Ta_6^+ cluster are well in line with a previous study.[56] Beyond that study, we went on and modeled the stepwise adsorption of N_2 molecules to the favored octahedral Ta_6^+ structure.

The slightly compressed octahedron provides for two distinguishable adsorption sites of likely end-on coordinated N_2 molecules, with either of the two polar Ta sites of the octahedron proving most favorable (cf. Table S4, isomer a). Note that the compression-distortion of the octahedral cluster did receive slight changes from the polar N_2 adsorption. In such (6,1), comprising a polar N_2 adsorbate, the prior equal equatorial bonds elongate (+0.10 Å) and compress (−0.12 Å) in concert with a minor tilting of 2° of the N_2 ligand with respect to the polar symmetry axis. This, in turn, makes the four equatorial Ta sites pairwise distinguishable. Alternatively, an N_2 adsorption onto either of the other four equatorial Ta centers (cf. Table S4, isomer b) would stabilize less, by +7 kJ/mol, and the according quartet states even less, +22 and +17 kJ/mol, respectively. Spin states seem to persist upon N_2 adsorption in the present case, and any spin raise seems unlikely. This is even more so in view of our spin-valley curves of the Ta_5^+ cluster species (5,m) (see above) and of several prior studies of adsorbate induced spin quenching in other TM clusters.[61,64] From here on, we constrain ourselves to consider doublet states of (6,m).

29 April 2024 14:10:59

© Author(s) 2023

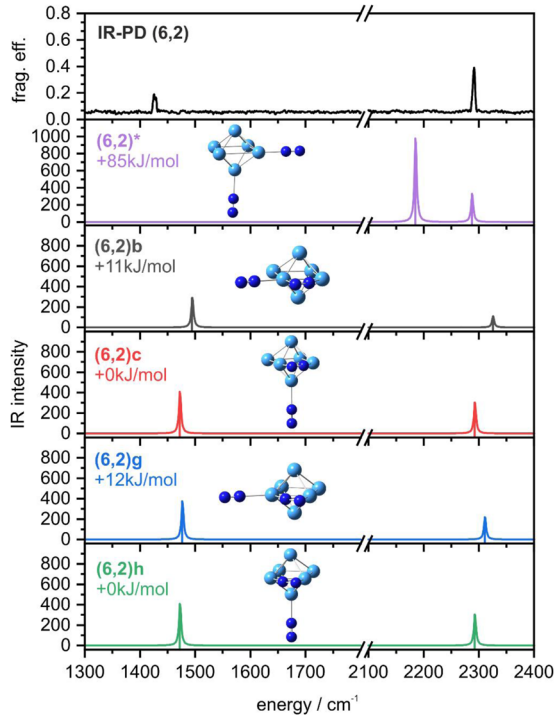

FIG. 4. Experimental IR-PD spectrum of (6,2) and DFT modeled spectra of selected structural isomers in the doublet state, their relative energies indicated with respect to the most stable isomer (6,2)c and the optimized cluster adsorbate structures. The predicted IR frequencies are scaled by a factor of 0.9586. For calculated energies and IR frequencies of all modeled isomers of (6,2), see Tables S6(b) and S7(b).

The recorded IR-PD bands of the (6,2) cluster complex at 1425 cm^{-1} motivate a computational quest for either of two N_2 molecules coordinating in a side-on (μ_2-κN:κN,N) motif. Indeed, such a motif proved more favorable by at least +85 kJ/mol [cf. Fig. 4 and Table S6(b)], than that of mere end-on coordination, whose predicted IR spectrum deviates from the measured IR-PD spectrum anyway (cf. Fig. 4). The identified most stable isomers (6,2)c and (6,2)h both comprise a side-on μ_2-κN:κN,N N_2 ligand that is coordinated to two equatorial Ta centers, next neighbors to the polar N_2 end-on coordinating Ta center (cf. Fig. 4). They differ by chirality, and they are degenerate, as expected [cf. Table S6(b) in the supplementary material]. The bond of the side-on N_2 coordinating Ta pair shortens by −0,07 Å (cf. Table S9).

We identified further $N_{2(side\text{-}on)}/N_{2(end\text{-}on)}$ ligand combinations, and we found them less stable by +11 to +20 kJ/mol. [cf. Tables S6(b) and S7(b)]. Obviously, both N_2 ligands seek proximity, and they benefit from a cooperative gain on the order of up to 20 kJ/mol in achieving such proximity. Indeed, our modeling confirms that the most stable degenerate isomer pairs [isomers (6,2)b/g and (6,2)c/h] reveal identical IR spectra, respectively. Moreover, all four IR spectra match the recorded IR-PD spectra (Fig. 4). In contrast, the computed IR spectra of the isomer pair (6,2)e,j, and further ones do not coincide with the recorded IR-PD spectrum [cf. Table S6(b)]. Most notably, it shows that the side-on N_2 orientation proves negligible, and hence, only the location of the coordinating Ta pair over which the side-on ligand is located is more relevant for searching for a matching minimum structure for the measured (6,2) IR-PD spectrum. The orientation of the side-on ligand over the edge seems to be less relevant. Furthermore, we have identified a cooperative effect between the end-on N_2 and the side-on N_2.

In order to model the observed stepwise uptake of a third N_2 ligand by Ta_6^+, we added a second end-on bound N_2 ligand to the prior end-on and side-on μ_2-κN:κN,N N_2 ligands [cf. Tables S6(c1) and S7(c1)]. It emerges from a favorable arrangement of the two end-on N_2 ligands at Ta centers on the opposite Ta corners of the octahedral core [cf. Fig. 5, structures (6,3)j and (6,3)w]. Both end-on N_2 ligands are located at distal coordination sites. The side-on μ_2-κN:κN,N N_2 ligand is located in between and proximal to either end-on N_2 ligand. The orientation of the side-on N_2 ligand across its coordinating Ta–Ta edge is degenerate. By virtue of the high symmetry, the modeled IR spectrum provides for merely two bands that match well the observed IR-PD bands at 2289 and 1468 cm^{-1}. Furthermore, observed IR-PD bands at 1416, 1625, and 2255 cm^{-1} point towards other isomers.

Up to now, we have not yet succeeded in identifying such candidates that would provide for two end-on and a single side-on ligand [cf. Fig. 5 and Fig. S7 (a)], and we wonder about some isomer with another degree of tilting of the N_2 side-on ligand. Note

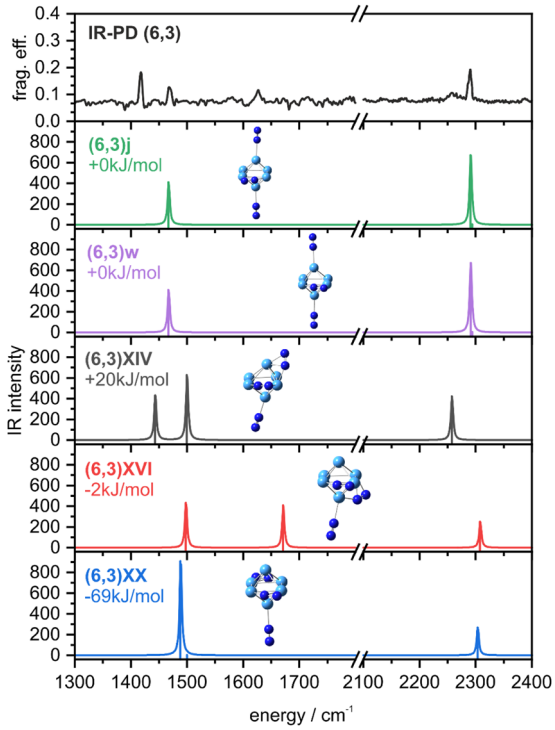

FIG. 5. Experimental IR-PD spectrum of (6,3) and DFT modeled spectra of selected structural isomers in the doublet state, their relative energies indicated with respect to isomers (6,3)j/w, and optimized cluster adsorbate structures included as insets. The predicted IR frequencies are scaled by a factor of 0.9586. For calculated energies and IR frequencies of all modeled isomers of (6,3), see Tables S6(c) and S7(c).

29 April 2024 14:10:59

© Author(s) 2023

that our adjoined study of Ta_4^+ [**IRS1**] confirms such effects. We find support for our hypothesis by a closer look at the bond distances $Ta_{\kappa(N,N)}$-$N_{side\text{-}on(\mu1)}$ and the angles $Ta_{\kappa(N,N)}$-$Ta_{\kappa(N)}$-$N_{side\text{-}on(\mu1)}$ of the twenty-two isomers at hand (6,3)a-w. Indeed, there is a correlation between an increase in the tilt of the side-on μ_2-κN:κN,N N_2 ligand and the observed redshift of its IR-PD vibrational frequency (cf. Table S8). This correlation seems independent of cluster size and cluster core structure, and it seems that the local Ta-(N–N)–Ta geometry dominates the observed effects.

In order to assign the IR-PD bands at 1416, 1625, and 2255 cm^{-1}, we consider isomers with two side-on μ_2-κN:κN,N N_2 adsorbates. Our modeling of several conceivable arrangements [cf. Tables S6(c) and 6(c)] yielded three isomers (6,3)XIV, (6,3)XVI, and (6,3)XX with a bunch of IR frequencies that agree quite well with the experimental IR-PD bands [cf. Fig. 5 and Fig. S7 (b)]. Within these three isomers, the arrangement of the end-on ligand and one of the side-on ligands corresponds to the structure of the most favorable isomer (6,2), as described earlier. Differences arise from varying positions of the second side-on ligand.

In the two isomers (6,3)XIV and (6,3)XVI, all three N_2 ligands are located in proximity to each other, and they share common Ta sites for coordination. These two isomers suffice to interpret all five experimental IR-PD bands at 1416, 1468, 1625, 2255, and 2289 cm^{-1} (cf. Fig. 5 and Fig. S7). The third isomer (6,3)XX, which is actually the most stable one at −69 kJ/mol, manages to locate its three N2 ligands while avoiding shared Ta sites.

This yields a highly symmetric arrangement of the N_2 ligands, and it causes merely a single IR band in the side-on range and merely another single IR band in the end-on range. Both match the experimental IR-PD bands at 1468 and 2289 cm^{-1}. Note that this isomer (6,3)XX on its own does not explain all observed IR-PD bands. However, we interpret the recorded IR-PD spectrum of (6,3) in terms of likely isomers (6,3) XIV and XVI, and we acknowledge possible contributions from other isomers.

In summary, DFT modeling provided insights into the structure of the first three adsorbate species (6,1), (6,2), and (6,3) on the Ta_6^+ cluster octahedron. The first N_2 ligand yielding (6,1) adsorbs most likely end-on to the cluster core followed by two N_2 adsorption steps giving two μ_2-κN:κN,N N_2 ligands in (6,3). This sequence of end-on adsorption before side-on adsorption of the first three N_2 ligands differs from the results of N_2 adsorption on the Ta_4^+ cluster (cf. Fries *et al.*[1] and the adjoined study [**IRS1**]) and highlights once more the differential behavior between cluster sizes Ta_n^+, $n \leq 4$, and Ta_n^+, $n \geq 5$.

At this point, we want to address the question of whether the DFT predictions and the recorded IR-PD spectra are in line with the recorded adsorption kinetics (cf. supplementary material, Text S9, Fig. S22). The kinetics show an N_2 adsorption cascade to the bare Ta_6^+ cluster. The possible isomers for (6,1), (6,2), and (6,3) identified by DFT modeling correspond in structure/geometry to this chain of successive N_2 adsorption steps. The isomer identified as most likely to be populated in each case serves as the initial geometry for the adsorption of the next N_2 molecule.

$[Ta_7(N_2)_m]^+$

From our kinetic studies presented and discussed in the supplementary material (cf. Text S10, Fig. S23), we know that the

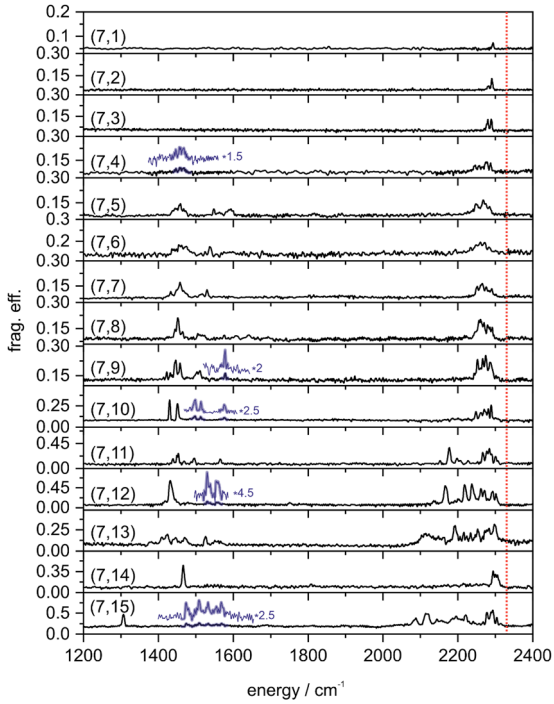

FIG. 6. IR-PD spectra of sequentially increasing cluster N_2 adsorbate complexes $[Ta_7(N_2)_m]^+$, m = 1–15, as recorded after prior 26 K He buffer gas cooling. Note the significant red-shift of the IR-PD bands with respect to the free N_2 stretching vibrational frequency (2330 cm^{-1},[76] red dotted line).

Ta_7^+ cluster adsorbs up to 16 N_2 molecules onto its cluster surface. We found an equilibrium between adsorbed species (7,10) to (7,16) at long reaction times. However, (7,16) is a very small, low-intensity product in equilibrium. Therefore, (7,15) became the largest N_2 adsorbate complex in our current IR-PD study of N_2 adsorption on Ta_7^+ (cf. Fig. 6). As before, we searched for IR-PD induced bands in the 1200 to 2400 cm^{-1} range and found numerous vibrational bands in two frequency ranges: below 2000 cm^{-1} for N_2 oscillators binding in a side-on μ_2-κN:κN,N motif to the Ta_7^+ cluster core, and beyond 2000 cm^{-1} for those binding end-on to single Ta centers. In the following, we discuss the experimental IR-PD spectra of the species in detail.

The N_2 adsorption chain on Ta_7^+ starts with the initial adsorbate species (7,1). For this species, we observe a single IR-PD band at 2294 cm^{-1} and thus a redshift with respect to the free N_2 stretching oscillation of −36 cm^{-1}. Once more, it seems reasonable to explain this redshift by a σ-donor and π-acceptor synergism. The presence of this IR-PD band provides strong evidence that spontaneous N_2 cleavage by Ta_7^+ does not proceed. Instead, Ta_7^+ appears to continue the trend that at a cluster size of n = 5 and beyond, adsorption of the first N_2 molecule occurs in end-on orientation to the cluster core and without further activation.

There are strong similarities in the IR-PD spectra of the subsequent two adsorbate species (7,2) and (7,3). Both spectra reveal a doublet with a splitting of 9 cm^{-1}: at 2282 and 2291 cm^{-1} for (7,2) and at 2280 and 2289 cm^{-1} for (7,3), respectively. The second

29 April 2024 14:10:59

© Author(s) 2023

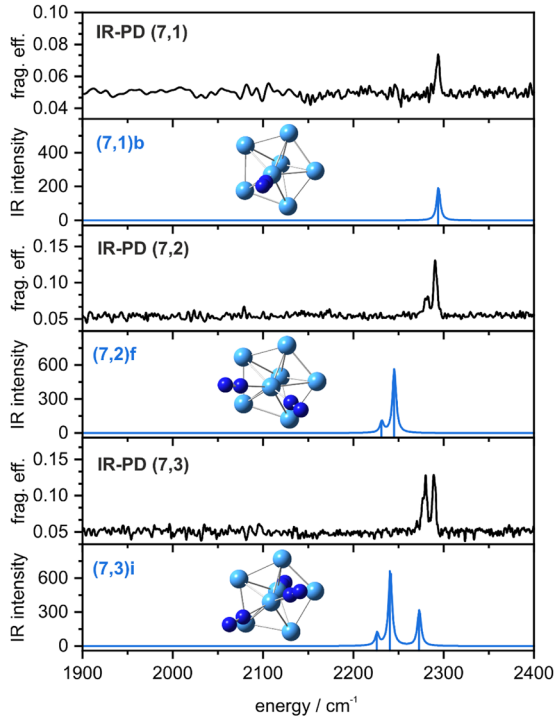

FIG. 7. Experimental IR-PD spectra of (7,1), (7,2), and (7,3) and DFT modeled spectra of selected structural isomers in the triplet state and the corresponding optimized cluster adsorbate structures as insets. The predicted IR frequencies are scaled by a factor of 0.9586. For calculated energies and IR frequencies of all modeled isomers of (7,m), see Tables S11(a)–S11(c) and S12(a)–S12(c).

N_2 molecule adsorbs to a site of the cluster such that another IR-PD band arises. A detailed examination of the (7,3) spectrum shows a very weak IR-PD sideband at 2277 cm^{-1} (Fig. 7). Our DFT modeling will reveal conceivable geometries and vibrational modes that will help to clarify.

For all of the species from (7,4) to (7,10), we observe a similar IR-PD band pattern in the end-on range above 2000 cm^{-1}. These spectra reveal induced fragmentation from 2234 cm^{-1} [the lowest end-on IR-PD fingerprint in the case of species (7,6)] to 2292 cm^{-1} [the highest end-on IR-PD fingerprint in the case of species (7,8)]. The number count of clearly identifiable IR-PD bands in the respective range varies between four and six.

The experimental IR-PD band patterns in the side-on region below 2000 cm^{-1} vary somewhat by the N_2 load, but they also show some recurring band patterns. For the adsorbate species (7,4), we observe a broad and weak IR-PD band around 1457 cm^{-1} with some partially resolved band structure. The IR-PD spectrum of the next larger adsorbate complexes (7,5) and beyond reveals a much more complex band pattern of side-on N_2 oscillators. Instead of a single broad IR-PD band around 1457 cm^{-1} (7,4), we now observe up to three bands for (7,5), (7,6), (7,7), and (7,8), which partially overlap and reveal some variation in their width but little shifts. This trend does not continue for the adsorbate species (7,9) and (7,10); instead, the spectra of both species show four and merely two sharp bands, respectively, all of which reveal clearly less bandwidth than the smaller adsorbate species.

In addition, for (7,5) and beyond, we observe some IR-PD adsorptions at up to 1600 cm^{-1}: There is some side-on N_2 stretching doublet structure that shifts to the red with N_2 load from 1548 to 1563 cm^{-1} in (7,5) to 1498 and 1513 cm^{-1} in (7,10). The IR-PD spectra of (7,5), (7,9), and (7,10) reveal an additional single band just below 1600 cm^{-1}, which also shifts to the red with N_2 load, from 1594 in (7,5) to 1576 cm^{-1} in (7,10).

With the adsorption of the eleventh N_2 molecule onto the cluster adsorbate complex, the range of the end-on IR-PD band pattern successively expands to the red, down to 2100 cm^{-1} in (7,13). Within this range, the IR-PD spectra of the three species (7,11), (7,12), and (7,13) show an average of ten bands, which is twice as much as for the previous adsorbate species (7,4) to (7,10).

In the side-on region below 2000 cm^{-1}, the adsorption of the eleventh N_2 preserves the band pattern of the (7,10) species, and the same largely holds for (7,13). In contrast, the IR-PD spectra of the species (7,12) reveal particularly different IR-PD fingerprints: There is a single intensive band at 1431 cm^{-1}, which is accompanied by some weak bands at 1530 and 1554 cm^{-1}. The occurrence of such a sharp and intense band indicates multiple side-on N_2 adsorbates in equivalent arrangements, likely μ_2-κN:κN,N type, that experience like next neighbor interactions and concomitant couplings of their stretching bands. Astonishing as it is, larger and smaller adsorbate complexes, namely (7,11) and (7,13), behave differently and provide for disliked next neighbor interactions among their side-on coordinated N_2 ligands.

The experimental IR-PD spectrum of the species (7,14) is conspicuous for its low number count of IR-PD bands. The (7,14) species provides for a formal N_2 double layer of two ligands per Ta site. If truly occupied in such a stoichiometric manner, it would provide for all equivalent ligands and high symmetry. Indeed, the IR-PD spectrum provides for a single intensive band at 1467 cm^{-1}, indicating side-on μ_2-κN:κN,N N_2 oscillators, and a single intensive broad band around 2301 cm^{-1}, originating from some end-on N_2 oscillators. It is thus clearly evident that the formal "double layer" species does provide for two types of clearly distinguishable N_2 adsorbates, with the exact count of each of them remaining undisclosed.

From (7,4) to (7,13), the number of measured IR-PD bands corresponded to or even exceeded the number of adsorbed N_2 molecules, which indicates the likely presence of multiple isomers of these species. In contrast, the IR-PD band number count of species (7,14) strongly suggests the occurrence of a single isomer.

It is surprising to recognize the positions and number count of the IR-PD bands of (7,15). There are at least twelve distinguishable adsorption maxima in the end-on range between 2088 and 2304 cm^{-1}. Even more surprisingly, the prior intense IR-PD band of (7,14) at 1467 cm^{-1} shifts by adsorption of the 15th N_2 ligand down to 1307 cm^{-1}, by as much as −160 cm^{-1}, which is quite significant. Some more weak bands arise between 1475 and 1568 cm^{-1}.

The recorded IR-PD spectra of (7,m) reveal numerous bands that provide information about the structure of the coordinated N_2 ligands within the respective cluster adsorbate complexes. The spectra of the first three adsorbate species, (7,1) to (7,3), indicate N_2 oscillators that bind end-on to single Ta centers. From (7,4) and beyond, we find evidence for N_2 oscillators binding in a side-on

29 April 2024 14:10:59

© Author(s) 2023

μ_2-κN:κN,N motif to the Ta_7^+ cluster core. We recognize the large number of IR-PD bands below 2000 cm^{-1}. Together with the IR-PD bands above 2000 cm^{-1}, the total number of IR-PD bands for all species from (7,4) and beyond, but (7,12) and (7,14), exceeds the number of N_2 oscillators of the respective cluster adsorbates. We take this as strong evidence for several co-existing adsorbate isomers. However, there is the case of (7,14), where the number of IR-PD bands clearly falls below the number of adsorbed N_2 ligands. This in turn indicates a highly symmetric arrangement of the N_2 ligands on the Ta_7^+ cluster framework within the formal double layer of N_2 oscillators.

In order to gain deeper insights into the N_2 adsorption on the Ta_7^+ cluster and the involved structures of the cluster adsorbate complexes, we performed DFT modeling of conceivable geometries.

First of all, we wondered about the bare framework of the Ta_7^+ cluster. We chose four geometries as starting points: a capped octahedron (coh), a pentagonal bipyramid (pbp), and two types of capped trigonal prism (ctp1: capped over square plane, ctp2: capped over triangle plane). The pentagonal bipyramid (pbp) in a triplet state turned out to be the most stable (cf. Table S10). Our conclusions on this naked Ta_7^+ cluster are well in line with a previous study.[56] Singlet and quintet states of the same geometry are less stable by +35 and +37 kJ/mol, respectively. As listed in the supplement (cf. Table S10), all other investigated geometries are less stable, e.g. +162 kJ/mol for the capped octahedral (^{3}coh) geometry. We, therefore, take the pentagonal bipyramidal (pbp) geometry for the Ta_7^+ framework as a starting point to investigate N_2 adsorption.

The highly symmetric pentagonal bipyramidal core structure of Ta_7^+ provides two distinguishable binding sites for the adsorption of a first N_2 molecule in end-on orientation. DFT modeling predicts that the two preferred triplet structures differ by 11 kJ/mol [cf. Tables S11(a) and S12(a)]. N_2 adsorption on one of the two tips of the pentagonal bipyramid is preferred as compared to adsorption on one of the Ta atoms of the pentagonal plane of the framework. The predicted IR band of the end-on N_2 oscillator comes close to the single experimental IR-PD band at 2294 cm^{-1} (cf. Fig. 7 and Fig. S8).

DFT modeling of conceivable geometries of species (7,2) [cf. Tables S11(b) and S12(b)] yielded merely a single isomer whose predicted IR band pattern matches the experimentally observed twin IR-PD bands at 2282 and 2291 cm^{-1} (cf. Fig. 7 and Fig. S8) but for some shift. The characteristic splitting of the IR-PD band results from an arrangement of both N_2 oscillators onto a single Ta atom. In consistency with the most stable isomer (7,1)b, which might serve as a precursor to this isomer (7,2)f, both N_2 molecules adsorb to either of the two tips of the pentagonal bipyramid. Unfortunately, this (7,2) isomer with this arrangement of N_2 ligands is 29 kJ/mol less stable than the most stable one in our DFT study. Nevertheless, we take this isomer to be the most likely, and we presume unknown issues on the DFT modeling side.

For species (7,3), our DFT modeling yields several isomers that differ in stability by a mere 19 kJ/mol [cf. Tables S11(c) and S12(c)]. None of the predicted IR band patterns reveal satisfactory predictions. The third most stable isomer (+6 kJ/mol) shows some resemblance with the observed IR-PD spectrum of (7,3) (cf. Fig. 7 and Fig. S9). In this isomer, the three N_2 oscillators would be distributed over the two tips of the pentagonal bipyramid. At this point, it becomes obvious that DFT modeling with our methods at hand reaches its limits, and we look very much forward to seeing other researcher pick up this topic, hopefully in the near future.

In summary, we conclude from our DFT modeling for conceivable geometries of the bare Ta_7^+ cluster (7,0) and of the first three adsorbate species (7,1), (7,2), (7,3) that the N_2 molecules adsorb in an end-on motif to the pentagonal bipyramid prior to an adsorption to one of the five Ta atoms forming the pentagonal plane of the framework.

At this point, our IR-PD spectra and our concomitant DFT modeling strongly suggest a consecutive uptake of N_2 adsorbates into end-on coordination geometries onto a presumed most stable Ta_7^+ isomer without any indication of its scaffold to rearrange or the spin states to relay. These findings are much in line with our kinetic studies of N_2 adsorption to Ta_7^+, as documented in the supplementary material (cf. Text S10, Fig. S23). There, we do observe stepwise N_2 uptake by the Ta_7^+ cluster, and we managed to perform a pseudo-first-order kinetic fit that does not indicate neither any isomerization nor any activation throughout the first four N_2 adsorption steps. The second and third N_2 adsorption processes proceed somewhat slower than the first step. This might correspond to the reasonable conclusion of sterically limited N_2 adsorption to the tips of the pentagonal bipyramidal framework of the Ta_7^+ cluster core.

The almost abrupt increase in the number of IR-PD bands from (7,4) and beyond, which we interpret as a clear indication of the presence of multiple isomers for each of the species, coincides with the increasing desorption rates from $k_{-(7,4)}$ on and beyond. Therefore, the isomers for all species from (7,4) onward appear to adsorb additional N_2 molecules with likely simultaneous isomerization of the adsorbate shell. There is further coincidence of a particular feature in the (7,11)th IR-PD spectra with the kinetics (cf. supplementary material, Fig. S23) of the eleventh N_2 adsorption onto Ta_7^+: The IR-PD spectrum of (7,11) reveals a significant extension of the end-on coordinated IR-PD bands to the red, and the recorded N_2 adsorption kinetics demonstrate an equilibrium of all cluster adsorbates from (7,10) and beyond. Therefore, our IR-PD studies and our kinetic studies come to the same conclusions. The increase in multiple N_2 coordination at the same tantalum centers causes likely isomerization, e.g., N_2 adsorbate site hopping.

$[Ta_8(N_2)_m]^+$

The Ta_8^+ cluster is the largest one that we characterized by recording the IR-PD spectra of (8,m), m = 1–8 (Fig. 8 and Fig. S10). We found no IR induced fragmentation in the low wavenumber range below 2000 cm^{-1} and, therefore, we have no indications for the formation of side-on μ_2-κN:κN,N coordinated N_2 oscillators in the investigated cluster adsorbate complexes. We observe several IR-PD bands above 2000 cm^{-1}, which likely stem from μ_1 end-on coordinated N_2 ligands of the Ta_8^+ cluster. The low yields of higher loaded adsorbate species (m > 8, cf. Fig. S25, supplementary material) hampered the recording of their IR-PD spectra, and the obtained signal-to-noise ratio is meager. Once more, it seems reasonable to assume weak σ-donation and considerable π-acceptance at work.

We observe a strong IR-PD band at 2261 cm^{-1} and a very weak band at 15 cm^{-1} to the blue, which indicates a second less likely isomer. With the current DFT modeling at hand, we cannot assign

29 April 2024 14:10:59

© Author(s) 2023

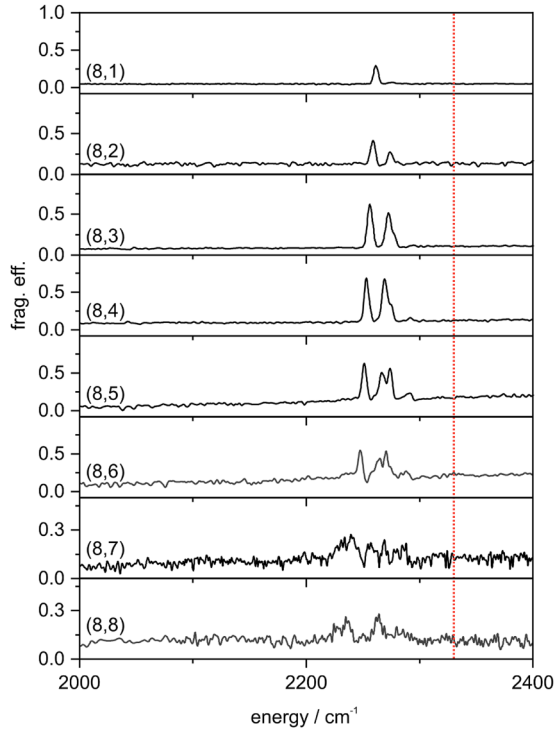

FIG. 8. IR-PD spectra of sequentially increasing cluster N_2 adsorbate complexes $[Ta_8(N_2)_m]^+$, m = 1–8, as recorded after prior 26 K He buffer gas cooling. Note the significant red-shift of the IR-PD bands with respect to the free N_2 stretching vibrational frequency (2330 cm^{-1},[76] red dotted line). For IR-PD spectra in the range of 1200–2400 cm^{-1}, see Fig. S10 in the supplementary material.

particular geometries to these isomers. We are left with the speculation that some coordination isomers form, which finds some support in our kinetic studies (cf. supplementary material, Text S11, Figs. S24 and S25). It is noteworthy to emphasize at this point that the presence of end-on coordinated N_2 fingerprinting IR-PD bands is a compelling argument for the lack of N_2 cleavage ability of the Ta_8^+ cluster.

The IR-PD band pattern of (8,1) persists in the IR-PD spectrum of (8,2), slightly shifted to 2259 and 2274 cm^{-1}. The latter one intensifies significantly. With the adsorption of the third N_2 molecule onto the Ta_8^+ cluster, this very IR-PD band pattern is preserved in (8,3), but for some shoulder of the blue band.

The species (8,4) reveals two intensive IR-PD bands at 2253 and 2269 cm^{-1}. The vaguely discernible blue shoulder of (8,3) has evolved into a clear feature of (8,4) at 2274 cm^{-1}. In addition, one notes a weak IR-PD band at 2292 cm^{-1}. It is this band pattern that persists in the IR-PD spectrum of (8,5) but with some intensity variations and minor shifts.

Besides an inferior signal-to-noise ratio, the (8,5) IR-PD bands persist in (8,6), and an additional band arises at 2241 cm^{-1}, which is to the red of all previous (8,m) bands. We found such behavior in (5,m), (6,m), and (7,m) at some point as well. The IR-PD spectra of species (8,6), (8,7), and (8,8) reveal six to eight bands at similar locations.

The cross-reference to our cryo-kinetics study of N_2 adsorption on the Ta_n^+ cluster, n = 2–8, supplementary material, yields further insights. The kinetic curve of the first adsorbate species (8,1), Fig. S25, provides strong indications for two isomers, which signify their different reactivity. Our interpretation of the IR-PD spectrum (8,1) concludes as well that there are two isomers, one of which is less populated.

CONCLUSION

We present an IR-PD study of tantalum cluster adsorbate complexes $[Ta_n(N_2)_m]^+$, abbreviated (n,m), n = 5–8, [**IRS2**], and in the adjoined IR-PD study [**IRS1**], we present findings for the N_2 adsorption to the smaller cluster adsorbate complexes $[Ta_{2\text{-}4}(N_2)_m]^+$.

We found numerous bands in the IR-PD spectra of species (5,m), m = 1–13, which are located mainly in the end-on coordinated N_2 stretching range. Some of these species (m = 9–12) indicate weak IR-PD signals, which we assign to side-on μ_2-κN:κN,N N_2 ligands. DFT calculations allowed us to tentatively assign cluster structures on the basis of trigonal bipyramidal (tbp) cluster cores. The evaluation of spin valley curves allows us to evaluate the spin-state-dependent stability of cluster adsorbate complexes in the course of N_2 adsorption. Triplet and singlet isomers reveal themselves to be most stable in all cases. We assume some spin quenching from triplet to singlet states upon adsorption of the fifth to tenth N_2 molecule. It is the subject of ongoing work to conduct extensive quantum chemical modeling of the seemingly hindered reaction path of (5,1) and of all of the stationary points.

We found numerous IR-PD bands of the N_2 adsorption species (6,m), m = 1–15, in two spectral ranges, 1400 to 1650 cm^{-1} and 2000 to 2310 cm^{-1}. DFT modeling revealed a sequence of initial N_2 end-on coordination and a subsequent mix of N_2 side-on adsorption. The recorded IR-PD spectra of (7,m) reveal numerous bands indicating N_2 oscillators that bind end-on to single Ta centers in complexes (7,1) to (7,3). From (7,4) on and beyond, we find evidence for N_2 oscillators binding in a side-on μ_2-κN:κN,N motif to the Ta_7^+ cluster core. We observe several IR-PD bands of (8,m), which likely stem from μ_1-end-on coordinated N_2 ligands. Starting from a few single and distinguishable end-on N_2 bands of the less occupied adsorbate complexes (n,m), n = 5–7, we observe a general increase in spectral complexity and an inhomogeneous broadening of bands, mainly towards the red, at certain points of N_2 loading m. We attribute this observation to an increasingly higher amount of double and triple N_2 coordination of Ta sites, eventually at all of them. The more N_2 ligands coordinate with single Ta sites, the more the vibrational frequencies shift to the red.

Other than the IR-PD spectra of the small tantalum clusters Ta_n^+, n = 2–4 (cf. Fries *et al.*[1] and the adjoined study [**IRS1**]), the present IR-PD spectra of the initial adsorbate species (n,1), n = 5–8, provide strong evidence for a lack of spontaneous N_2 cleavage. Instead, there are significant IR-PD fingerprints of end-on bound N_2 molecules on otherwise bare Ta_n^+, n = 5–8, clusters throughout. It appears as if an enhanced entrance channel barrier prevents spontaneous tilting and further activation. In the cases of n = 5–8, it takes further N_2 adsorption to find some weak side-on μ_2-κN:κN,N N_2 fingerprints, and the reasoning for the onset of these features at (5,9), (6,2), and (7,4) is an open question as of now. One

29 April 2024 14:10:59

© Author(s) 2023

may speculate on a conceivable N_2–N_2 cooperativity that is highly sensitive to cluster surface morphologies and thereby also to the cluster sizes. In any case, it is a sound finding that the spontaneous N_2 cleavage by Ta_n^+, n = 5–8, is suppressed. Therefore, the ability of a small Ta cluster to cleave dinitrogen (cf. Fries *et al.*[1] and [**IRS1**]) disappears by adding a single, fifth metal atom to the cluster core.

The above-mentioned findings find strong support in our cryogenic kinetic studies, as documented in the supplementary material. There, we present a study of stepwise N_2 adsorption on size selected Ta_n^+, n = 5–8 clusters, yielding $[Ta_n(N_2)_m]^+$. The N_2 adsorption reaches a limit $m_{(max)}$ = 16, which does not depend on cluster size n, and we observe a final equilibrium among those adsorbate complexes that possess up to three to five N_2 adsorbates less than $m_{(max)}$, and the kinetic fits revealed significant N_2 desorption rates upon higher N_2 loads. The variations of absolute rates find reasonable interpretation in terms of simple thermodynamic arguments. We find some evidence for spin quenching, and it mixes in a conceivable coexistence of isomeric cluster adsorbate complexes.

SUPPLEMENTARY MATERIAL

Online supplementary material comprises a nomenclature for the clusters and their adsorbates, comprehensive listings of energetics, structures, and IR frequencies of computed structures, further experimental and computed IR spectra, and multiple text blocks and viewgraphs on the conducted kinetic experiments, kinetic fits, and their interpretation in detail.

ACKNOWLEDGMENTS

This work was supported by the German research foundation DFG within the trans-regional collaborative research center Grant No. SFB/TRR 88 (Cooperative effects in homo and heterometallic complexes, 3MET.de) and by the research center OPTIMAS. We acknowledge Thomas Kolling for his technical assistance and valuable discussion. Quantum chemical modeling took place at the "Regionales Hochschulrechenzentrum Kaiserslautern" (RHRK).

AUTHOR DECLARATIONS

Conflict of Interest

The authors have no conflicts to disclose.

Author Contributions

The experiments were performed by D.V.F.—partly together with A.S., M.P.K., and M.E.H. D.V.F. and M.P.K. performed the quantum chemical calculations. The evaluation of the measured data was carried out by D.V.F., and it was accompanied by discussions with A.S., M.P.K., and G.N.-S. D.V.F. and G.N.-S. wrote the manuscript, which all the authors revised and agreed to.

Daniela V. Fries: Data curation (lead); Formal analysis (lead); Investigation (lead); Validation (equal); Writing – original draft (equal); Writing – review & editing (equal). **Matthias P. Klein**: Conceptualization (supporting); Data curation (supporting); Investigation (supporting); Methodology (supporting); Validation (supporting); Writing – review & editing (supporting). **Annika Straßner**: Data curation (supporting); Investigation (supporting); Methodology (supporting); Resources (supporting); Validation (supporting); Writing – review & editing (supporting). **Maximilian E. Huber**: Data curation (supporting); Formal analysis (supporting); Investigation (supporting); Project administration (supporting); Validation (supporting); Writing – review & editing (supporting). **Gereon Niedner-Schatteburg**: Conceptualization (lead); Formal analysis (equal); Funding acquisition (lead); Investigation (supporting); Methodology (lead); Project administration (lead); Resources (lead); Supervision (lead); Validation (equal); Writing – original draft (equal); Writing – review & editing (equal).

DATA AVAILABILITY

The data that support the findings of this study are available from the corresponding author upon reasonable request.

REFERENCES

[1] D. V. Fries, M. P. Klein, A. Steiner, M. H. Prosenc, and G. Niedner-Schatteburg, Phys. Chem. Chem. Phys. **23**(19), 11345–11354 (2021).
[2] A. Mittasch, *Geschichte der Ammoniaksynthese* (Verlag Chemie, 1951).
[3] K. Ziegler, H. Breil, E. Hilzkamp, and H. Martin, Germany Patent No. DE973626C (14 April 1960).
[4] W. Ostwald, United Kingdom Patent No. GB190200698A (20 March 1902).
[5] BASF, Germany Patent No. DE235421C (13 October 1908).
[6] F. Fischer and H. Tropsch, Germany Patent No. DE524468C (7 May 1931).
[7] F. Fischer and H. Tropsch, Germany Patent No. DE484337C (16 October 1929).
[8] H. S. Taylor, Proc. R. Soc. London, Ser. A **108**(745), 105–111 (1925).
[9] S. M. Lang and T. M. Bernhardt, Phys. Chem. Chem. Phys. **14**(26), 9255–9269 (2012).
[10] D. K. Böhme and H. Schwarz, Angew. Chem., Int. Ed. **44**(16), 2336–2354 (2005).
[11] R. A. J. O'Hair and G. N. Khairallah, J. Cluster Sci. **15**(3), 331–363 (2004).
[12] P. Armentrout, Annu. Rev. Phys. Chem. **52**(1), 423–461 (2001).
[13] M. M. Kappes, Chem. Rev. **88**(2), 369–389 (1988).
[14] P. B. Armentrout, Catal. Sci. Technol. **4**(9), 2741–2755 (2014).
[15] M. D. Morse, M. E. Geusic, J. R. Heath, and R. E. Smalley, J. Chem. Phys. **83**(5), 2293–2304 (1985).
[16] L.-H. Mou, Y. Li, Z.-Y. Li, Q.-Y. Liu, H. Chen, and S.-G. He, J. Am. Chem. Soc. **143**(45), 19224–19231 (2021).
[17] L.-H. Mou, Y. Li, G.-P. Wei, Z.-Y. Li, Q.-Y. Liu, H. Chen, and S.-G. He, Chem. Sci. **13**(32), 9366–9372 (2022).
[18] M. R. Zakin, D. M. Cox, and A. Kaldor, J. Chem. Phys. **87**(8), 5046–5048 (1987).
[19] G.-D. Jiang, L.-H. Mou, J.-J. Chen, Z.-Y. Li, and S.-G. He, J. Phys. Chem. A **124**(38), 7749–7755 (2020).
[20] C. Geng, J. Li, T. Weiske, and H. Schwarz, Proc. Natl. Acad. Sci. U. S. A. **115**(46), 11680–11687 (2018).
[21] C. Geng, J. Li, T. Weiske, and H. Schwarz, Proc. Natl. Acad. Sci. U. S. A. **116**(43), 21416–21420 (2019).
[22] F. Mafuné, Y. Tawaraya, and S. Kudoh, J. Phys. Chem. A **120**(24), 4089–4095 (2016).
[23] M. Kumar Yadav and A. Mookerjee, Physica B **405**(18), 3940–3942 (2010).
[24] J. F. Eckhard, T. Masubuchi, M. Tschurl, R. N. Barnett, U. Landman, and U. Heiz, J. Phys. Chem. C **122**(44), 25628–25637 (2018).
[25] J. Lengyel, N. Levin, F. J. Wensink, O. V. Lushchikova, R. N. Barnett, U. Landman, U. Heiz, J. M. Bakker, and M. Tschurl, Angew. Chem., Int. Ed. **59**(52), 23631–23635 (2020).

29 April 2024 14:10:59

© Author(s) 2023

[26]J. F. Eckhard, T. Masubuchi, M. Tschurl, R. N. Barnett, U. Landman, and U. Heiz, J. Phys. Chem. A **125**(24), 5289–5302 (2021).
[27]N. Levin, J. T. Margraf, J. Lengyel, K. Reuter, M. Tschurl, and U. Heiz, Phys. Chem. Chem. Phys. **24**(4), 2623–2629 (2022).
[28]J. F. Eckhard, D. Neuwirth, C. Panosetti, H. Oberhofer, K. Reuter, M. Tschurl, and U. Heiz, Phys. Chem. Chem. Phys. **19**(8), 5985–5993 (2017).
[29]R. Schlögl, Angew. Chem., Int. Ed. **42**(18), 2004–2008 (2003).
[30]H. Liu, Chin. J. Catal. **35**(10), 1619–1640 (2014).
[31]L. Geng, Y. Jia, H. Zhang, C. Cui, and Z. Luo, ChemPhysChem **23**(17), e202200288 (2022).
[32]C. Cui, Y. Jia, H. Zhang, L. Geng, and Z. Luo, J. Phys. Chem. Lett. **11**(19), 8222–8230 (2020).
[33]M. Zhou, X. Jin, Y. Gong, and J. Li, Angew. Chem., Int. Ed. **46**(16), 2911–2914 (2007).
[34]X. Cheng, Z.-Y. Li, L.-H. Mou, Y. Ren, Q.-Y. Liu, X.-L. Ding, and S.-G. He, Chem. – A Eur. J. **25**(72), 16523–16527 (2019).
[35]Y. Gong, Zhao, and M. Zhou, J. Phys. Chem. A **111**(28), 6204–6207 (2007).
[36]Z.-Y. Li, Y. Li, L.-H. Mou, J.-J. Chen, Q.-Y. Liu, S.-G. He, and H. Chen, J. Am. Chem. Soc. **142**(24), 10747–10754 (2020).
[37]Z.-Y. Li, F. Horn, Y. Li, L.-H. Mou, W. Schöllkopf, H. Chen, S.-G. He, and K. R. Asmis, Chem. Eur. J. **29**(14), e202203384 (2022).
[38]Y.-Q. Ding, Z.-Y. Chen, Z.-Y. Li, X. Cheng, M. Wang, and J.-B. Ma, J. Phys. Chem. A **126**(9), 1511–1517 (2022).
[39]M. C. Tsai, U. Ship, I. C. Bassignana, J. Küppers, and G. Ertl, Surf. Sci. **155**(2), 387–399 (1985).
[40]H. J. Freund, B. Bartos, R. P. Messmer, H. Grunze, H. Kuhlenbeck, and M. Neumann, Surf. Sci. **185**(1), 187–202 (1987).
[41]A. Fielicke, A. Kirilyuk, C. Ratsch, J. Behler, M. Scheffler, G. Von Helden, and G. Meijer, Phys. Rev. Lett. **93**(2), 023401 (2004).
[42]J. Oomens, B. G. Sartakov, G. Meijer, and G. von Helden, Int. J. Mass Spectrom. **254**(1), 1–19 (2006).
[43]J. R. Eyler, Mass Spectrom. Rev. **28**(3), 448–467 (2009).
[44]P. Maitre, D. Scuderi, D. Corinti, B. Chiavarino, M. E. Crestoni, and S. Fornarini, Chem. Rev. **120**(7), 3261–3295 (2020).
[45]J. Roithová, Chem. Soc. Rev. **41**(2), 547–559 (2012).
[46]G. Altinay and R. B. Metz, Int. J. Mass Spectrom. **297**(1-3), 41–45 (2010).
[47]B. Chiavarino, M. E. Crestoni, M. Schütz, A. Bouchet, S. Piccirillo, V. Steinmetz, O. Dopfer, and S. Fornarini, J. Phys. Chem. A **118**(34), 7130–7138 (2014).
[48]O. Dopfer, J. Phys. Org. Chem. **19**(8-9), 540–551 (2006).
[49]N. I. Hammer, J. W. Shin, J. M. Headrick, E. G. Diken, J. R. Roscioli, G. H. Weddle, and M. A. Johnson, Science **306**(5696), 675–679 (2004).
[50]J. M. Headrick, E. G. Diken, R. S. Walters, N. I. Hammer, R. A. Christie, J. Cui, E. M. Myshakin, M. A. Duncan, M. A. Johnson, and K. D. Jordan, Science **308**(5729), 1765–1769 (2005).
[51]A. M. Rijs and J. Oomens, Top. Curr. Chem. **364**, 1–42 (2015).
[52]T. R. Rizzo and O. V. Boyarkin, Top. Curr. Chem. **364**, 43–97 (2015).
[53]T. R. Rizzo, J. A. Stearns, and O. V. Boyarkin, Int. Rev. Phys. Chem. **28**(3), 481–515 (2009).
[54]W. H. Robertson and M. A. Johnson, Annu. Rev. Phys. Chem. **54**, 173–213 (2003).
[55]P. Gruene, A. Fielicke, and G. Meijer, J. Chem. Phys. **127**(23), 234307 (2007).
[56]J. Du, X. Sun, and G. Jiang, J. Chem. Phys. **136**(9), 094311 (2012).
[57]X. Sun and X. Huang, ACS Omega **7**(26), 22682–22688 (2022).
[58]L.-H. Mou, Z.-Y. Li, and S.-G. He, J. Phys. Chem. Lett. **13**(18), 4159–4169 (2022).
[59]J. Mohrbach, S. Dillinger, and G. Niedner-Schatteburg, J. Phys. Chem. C **121**(20), 10907–10918 (2017).
[60]S. Dillinger, J. Mohrbach, and G. Niedner-Schatteburg, J. Chem. Phys. **147**(18), 184305 (2017).
[61]A. A. Ehrhard, M. P. Klein, J. Mohrbach, S. Dillinger, and G. Niedner-Schatteburg, Mol. Phys. **119**(17-18), e1953172 (2021).
[62]A. A. Ehrhard, M. P. Klein, J. Mohrbach, S. Dillinger, and G. Niedner-Schatteburg, J. Chem. Phys. **156**(5), 054308 (2022).
[63]A. Straßner, M. P. Klein, D. V. Fries, C. Wiehn, M. E. Huber, J. Mohrbach, S. Dillinger, D. Spelsberg, P. B. Armentrout, and G. Niedner-Schatteburg, J. Chem. Phys. **155**(24), 244306 (2021).
[64]A. Straßner, C. Wiehn, M. P. Klein, D. V. Fries, S. Dillinger, J. Mohrbach, M. H. Prosenc, P. B. Armentrout, and G. Niedner-Schatteburg, J. Chem. Phys. **155**(24), 244305 (2021).
[65]S. Dillinger, J. Mohrbach, J. Hewer, M. Gaffga, and G. Niedner-Schatteburg, Phys. Chem. Chem. Phys. **17**(16), 10358–10362 (2015).
[66]S. Dillinger, M. P. Klein, A. Steiner, D. C. McDonald, M. A. Duncan, M. M. Kappes, and G. Niedner-Schatteburg, J. Phys. Chem. Lett. **9**(4), 914–918 (2018).
[67]M. P. Klein, A. A. Ehrhard, J. Mohrbach, S. Dillinger, and G. Niedner-Schatteburg, Top. Catal. **61**(1), 106–118 (2018).
[68]M. J. Frisch, G. W. Trucks, H. B. Schlegel, G. E. Scuseria, M. A. Robb, J. R. Cheeseman, G. Scalmani, V. Barone, B. Mennucci, G. A. Petersson, H. Nakatsuji, M. Caricato, X. Li, H. P. Hratchian, A. F. Izmaylov, J. Bloino, G. Zheng, J. L. Sonnenberg, M. Hada, M. Ehara, K. Toyota, R. Fukuda, J. Hasegawa, M. Ishida, T. Nakajima, Y. Honda, O. Kitao, H. Nakai, T. Vreven, J. A. Montgomery, Jr., J. E. Peralta, F. Ogliaro, M. Bearpark, J. J. Heyd, E. Brothers, K. N. Kudin, V. N. Staroverov, R. Kobayashi, J. Normand, K. Raghavachari, A. Rendell, J. C. Burant, S. S. Iyengar, J. Tomasi, M. Cossi, N. Rega, J. M. Millam, M. Klene, J. E. Knox, J. B. Cross, V. Bakken, C. Adamo, J. Jaramillo, R. Gomperts, R. E. Stratmann, O. Yazyev, A. J. Austin, R. Cammi, C. Pomelli, J. W. Ochterski, R. L. Martin, K. Morokuma, V. G. Zakrzewski, G. A. Voth, P. Salvador, J. J. Dannenberg, S. Dapprich, A. D. Daniels, Ö. Farkas, J. B. Foresman, J. V. Ortiz, J. Cioslowski, and D. J. Fox, GAUSSIAN 09, Revision E.01, *Gaussian, Inc.*, Wallingford, CT, 2009.
[69]M. J. Frisch, G. W. Trucks, H. B. Schlegel, G. E. Scuseria, M. A. Robb, J. R. Cheeseman, G. Scalmani, V. Barone, G. A. Petersson, H. Nakatsuji, X. Li, M. Caricato, A. V. Marenich, J. Bloino, B. G. Janesko, R. Gomperts, B. Mennucci, H. P. Hratchian, J. V. Ortiz, A. F. Izmaylov, J. L. Sonnenberg, D. Williams-Young, F. Ding, F. Lipparini, F. Egidi, J. Goings, B. Peng, A. Petrone, T. Henderson, D. Ranasinghe, V. G. Zakrzewski, J. Gao, N. Rega, G. Zheng, W. Liang, M. Hada, M. Ehara, K. Toyota, R. Fukuda, J. Hasegawa, M. Ishida, T. Nakajima, Y. Honda, O. Kitao, H. Nakai, T. Vreven, K. Throssell, J. A. Montgomery, Jr., J. E. Peralta, F. Ogliaro, M. J. Bearpark, J. J. Heyd, E. N. Brothers, K. N. Kudin, V. N. Staroverov, T. A. Keith, R. Kobayashi, J. Normand, K. Raghavachari, A. P. Rendell, J. C. Burant, S. S. Iyengar, J. Tomasi, M. Cossi, J. M. Millam, M. Klene, C. Adamo, R. Cammi, J. W. Ochterski, R. L. Martin, K. Morokuma, O. Farkas, J. B. Foresman, and D. J. Fox, GAUSSIAN 16, Revision C.01, *Gaussian, Inc.*, Wallingford, CT, 2016.
[70]J. P. Perdew, K. Burke, and M. Ernzerhof, Phys. Rev. Lett. **78**(7), 1396 (1997).
[71]C. Adamo and V. Barone, J. Chem. Phys. **110**(13), 6158–6170 (1999).
[72]F. Weigend and R. Ahlrichs, Phys. Chem. Chem. Phys. **7**(18), 3297–3305 (2005).
[73]D. Andrae, U. Häußermann, M. Dolg, H. Stoll, and H. Preuß, Theor. Chim. Acta **77**(2), 123–141 (1990).
[74]D. Figgen, K. A. Peterson, M. Dolg, and H. Stoll, J. Chem. Phys. **130**(16), 164108 (2009).
[75]E. D. Glendening, J. K. Badenhoop, A. E. Reed, J. E. Carpenter, J. A. Bohmann, C. M. Morales, and F. Weinhold, NBO 5.9, 2009.
[76]W. M. Haynes, *CRC Handbook of Chemistry and Physics* (CRC Press Taylor & Francis Group, 2014).
[77]M. P. Klein, Ph.D. thesis, Technische Universität Kaiserslautern, 2021.

29 April 2024 14:10:59

© Author(s) 2023